

K-Shell Photoabsorption of Magnesium Ions

M. F. Hasoğlu

Department of Computer Engineering, Hasan Kalyoncu University, 27100 Sahinbey,
Gaziantep, Turkey

Sh. A. Abdel-Naby

Department of Physics, Auburn University, Auburn, Alabama 36849

T. W. Gorczyca

Department of Physics, Western Michigan University, Kalamazoo, MI 49008-5252

Received _____; accepted _____

Not to appear in Nonlearned J., 45.

ABSTRACT

X-ray photoabsorption cross sections have been computed for all magnesium ions using the R -matrix method. A comparison with the other available data for Mg II-Mg X shows good qualitative agreement in general. However, for the lower ionization stages, and for singly-ionized Mg II in particular, the previous R-matrix results (Witthoeft et al. 2009; Witthoeft et al. 2011) overestimate the K-edge position due to the absence of important orbital relaxation effects in those earlier calculations, and a global shift downward in photon energy of those cross sections is therefore warranted. The resultant resonance shapes are found to be quite similar between the two R-matrix results, on the other hand. The cross sections for Mg I and Mg II are further complicated by the M-shell ($n = 3$) occupancy. As a result, the treatment of spectator Auger decay of $1s \rightarrow np$ resonances using the multichannel quantum defect, optical potential method becomes problematic, and it was necessary to implement an alternative, approximate treatment of Auger decay for neutral Mg I.

Subject headings: photoabsorption cross sections, magnesium ions

1. Introduction

Accurate K-shell photoabsorption cross sections are necessary for modeling astrophysical plasmas, interpreting the observed spectra from distant cosmic emitters, and determining the elemental abundances of the interstellar medium (ISM). Spectra of K-shell processes can be observed from all ionic stages of the most abundant elements between oxygen and nickel (Paerels & Kahn 2003). In previous studies, we have carried out K-shell photoabsorption calculations, and applied these data to X-ray spectral diagnostic studies, for all ionization stages of carbon (Hasoğlu et al. 2010), oxygen (Gorczyca & McLaughlin 2000; Garcia et al. 2005; Juett et al. 2004), and neon (Gorczyca 2000; Juett et al. 2006), i.e., for $Z = 6, 8$, and 10 , respectively. Here we continue those studies for all magnesium ions ($Z = 12$), which, although lower in abundance, nevertheless can be seen in X-ray absorption spectra (see Schulz et al. 2010; Pinto et al. 2010, for example).

For $Z = 12$, a further complication is introduced into the computations for the two lowest ionization stages (Mg I and Mg II), where the $n = 3$ M-shell becomes occupied: the atomic radius now doubles in size, and the usual multichannel quantum defect theory (MQDT) optical potential treatment (Gorczyca & Robicheaux 1999) becomes problematic for the lowest $1s \rightarrow np$ resonances. Nevertheless, we have come up with an approximate procedure for treating these cases as well, and we thus present reliable X-ray photoabsorption cross sections for all relevant magnesium ions (Mg I-Mg X).

2. Theoretical Methodology

K-shell photoabsorption consists of the direct photoionization of the $1s$ electron, which is treated in a straightforward manner using R-matrix methods, and the strong $1s \rightarrow np$ photoabsorption resonances. Photoexcitation of these resonance states is then followed by

two competing decay routes. The first is *participator* Auger decay, in which the valence electron np participates in the autoionization process, with a decay rate that scales as $1/n^3$ and goes to zero near the K-shell threshold. These channels are included in the R -matrix calculations. The second route is *spectator* Auger decay, in which the valence electron np does not participate in the autoionization process, giving instead a decay width that is independent of n . Therefore, it is the dominant decay route as $n \rightarrow \infty$ and guarantees a smooth cross section as the K-shell threshold is approached; above each threshold, K-shell photoionization to the $1s2\ell^q$ states occurs instead.

We use the R -matrix method (Berrington et al. 1995; Burke 2011), with modifications to account for the spectator Auger broadening via an optical potential approach as described by Gorczyca & Robicheaux (1999). This enhanced R -matrix method is shown to be successful in describing experimental synchrotron measurements for argon (Gorczyca & Robicheaux 1999), oxygen (Gorczyca & McLaughlin 2000), neon (Gorczyca 2000), and carbon (Hasoğlu et al. 2010). The Auger widths for the $1s2\ell^q$ states are computed by applying the Smith time-delay method (Smith 1960) to the photoabsorption R -matrix calculation of the neighboring $1s^22\ell^{q-1}$ magnesium ion. Further details can be found in our previous works (Gorczyca & Robicheaux 1999; Gorczyca & McLaughlin 2000; Gorczyca 2000; Hasoğlu et al. 2010).

3. Cross Section Results

As an assessment of the present atomic description, the computed target state energies and binding energies are presented in Tables 1-10, which show fairly good agreement with the recommended NIST values. The computed core Auger widths, which are used within the MQDT optical potential approach for treating spectator Auger broadening of resonances, are presented in Tables 11-19. Comparison with other available data shows

fairly good agreement in most cases, indicating again that the present atomic description is sufficient. It is to be noted that the spectator Auger width used in our calculations only changes the shape of the resonance absorption profile, not the strength.

In Figs. 2-10, we present our K-shell photoabsorption cross sections. Also shown in all the figures are the independent-particle (IP) photoionization results (Verner et al. 1993), and it is seen that the present R-matrix results are in good quantitative agreement with the IP results above the K-shell thresholds, but the IP cross sections lack the important resonance absorption lines below threshold.

In Fig. 1, we show the Mg I photoabsorption cross section, for which there are no other $1s \rightarrow np$ resonance cross sections available for comparison purposes. However, as can be deduced from Table 1, our K-shell threshold is computed as 1311.03 eV, in fairly good agreement with the experimental value of 1311.4 eV (Banna et al. 1982). Furthermore, since our above-threshold cross section is seen to align with the IP results, we have confidence in the below-threshold resonance oscillator strength, which should merge to the above-threshold oscillator strength density by continuity within the R-matrix calculations. Also shown in Fig. 1 are the solid-state experimental results of Henke et al. (1993). It is interesting to note that the present R-matrix results, for *neutral* Mg I, align more closely with the experimental results than with IP results, which do not include relaxation effects (but shift the threshold downward to align with experiment).

Of particular note regarding these R-matrix calculations for Mg I, it was not possible to apply the usual MQDT optical potential method (Gorczyca & Robicheaux 1999) for the spectator Auger broadening. This was because, due to the larger atomic radius, i.e., the R-matrix “box” (Berrington et al. 1995; Burke 2011), the energy dependence of the MQDT parameters at the lowest resonances invalidated the simple $E \rightarrow E + i\Gamma/2$ substitution (Gorczyca & Robicheaux 1999). Instead, a more rigorous approach, which is beyond the

scope of this paper, is necessary for the proper modeling of the Auger *width* (as noted before, the strength is not affected by the particular width used). In order to present reliable cross sections nevertheless, we use a spectator width which is small enough that the energy-dependent MQDT parameters can still be treated as constant over the width of a resonance, but large enough that the Rydberg series of resonances can be mapped out with a finite number of R-matrix energy points. These cross sections are then further convoluted with a Lorentzian profile of width 0.0254 eV (see Table 11) to simulate the known Auger broadening.

We turn now to ionized species of magnesium. The only other $1s \rightarrow np$ resonance cross sections we are aware of are those of Witthoeft et al. (2009) and Witthoeft et al. (2011), which were computed using a similar *R*-matrix method. However, important orbital relaxation effects were not included in those earlier R-matrix calculations. Relaxation is due to the sudden change in potential “seen” by the outer-most electrons following excitation or ionization of an inner-shell electron (the $1s$ electron, in this case), and the relative change in potential is greatest at the lowest ionization stages. Hence, the Mg II ion is expected to be the most affected by relaxation effects. Indeed, the K-shell threshold is seen to be overestimated by approximately 10 eV. This overestimate, due to the absence of relaxation effects, is seen to diminish, as the ionic charge increases, to the order of 2 eV, which would seem to indicate some lack of correlation, perhaps the strong $2p^2 \rightarrow \overline{3d}^2$ double promotions that require optimized $\overline{3d}$ pseudoorbitals as well.

4. Summary and Conclusion

In order to provide reliable X-ray absorption data near the magnesium K-edge, we have computed photoabsorption cross sections for Mg I-Mg X. We use an R-matrix method with the inclusion of spectator Auger decay, and treat both the $1s \rightarrow np$ resonance absorption

for all $n \rightarrow \infty$ and the above-threshold $1s \rightarrow \epsilon p$. We find good agreement with the IP data (Verner et al. 1993) for the above-threshold cross section.

Below threshold, the only other existing cross sections available for comparison purposes are the earlier R-matrix results of Witthoeft et al. (2009); Witthoeft et al. (2011) for the $1s \rightarrow np$ photoionization in Mg II-Mg X ions. In general, we find that our present results are in good qualitative agreement with the earlier R-matrix results regarding the resonance shapes. However, here we have included the important orbital relaxation effects, thereby obtaining reliable K-edge threshold positions, in much better agreement with experiment for Mg I.

Most importantly, we have provided a comprehensive set of magnesium photoabsorption data for the entire photon energy region including all $1s \rightarrow np$ resonances. These are broadened due to spectator Auger decay, and they merge smoothly onto the $1s \rightarrow \epsilon p$ above-threshold continuum. Thus the K-edge photoabsorption features are modeled correctly. These computed data are particularly important for interpreting observed X-ray spectra and determining ISM abundances.

5. Acknowledgment

This work was supported in part by a NASA APRA grant.

REFERENCES

- Banna, M. S., Slaughter, A. R., Mathews, R. D., Key, R. J., & Ballina, S. M. 1982, Chemical Physics Letters, 92, 122
- Berrington, K. A., Eissner, W., & Norrington, P. H. 1995, Comput. Phys. Commun., 92, 290.
- Burke, P. G. 2011, R-matrix Theory of Atomic Collisions (New York: Springer)
- Chen, M. H. 1985, Phys. Rev. A, 31, 1449.
- Chen, M. H. 1986, Atomic Data and Nuclear Data Tables, 34, 301.
- Chen, M. H. and Craseman, B. 1988, Atomic Data and Nuclear Data Tables, 38, 381
- Garcia, J., Mendoza, C., Bautista, M. A., Gorczyca, T. W., Kallman, T. R., & Palmeri, P. 2005, ApJS, 158, 68.
- Gorczyca, T. W., & Robicheaux, F. 1999, Phys. Rev. A, 60, 1216.
- Gorczyca, T. W., & McLaughlin, B. M. 2000, J. Phys. B: At. Mol. Opt. Phys., 33, L859.
- Gorczyca, T. W. 2000, Phys. Rev. A, 61, 024702.
- Gorczyca, T. W., et al. 2003, The Astrophysical Journal, 592, 636.
- Gorczyca, T. W., Dumitriu, I., Hasoğlu, M. F., Korista, K. T., Badnell, N. R., Savin, D. W., & Manson, S. T. 2006, ApJ, 638, L121.
- Hasoğlu, M. F., Gorczyca, T. W., Korista, K. T., Manson, S. T., Badnell, N. R., & Savin, D. W. 2006, ApJ, 649, L149.
- Hasoğlu, M. F., Nikolic, D., Gorczyca, T. W., Manson, S. T., Chen, M. H., & Badnell, N. R. 2008, Physical Review A, 78, 032509

- Hasoğlu, M. F., Abdel-Naby, Sh. A., Gorczyca, T. W., Drake, J. J., & McLaughlin, B. M. 2010, *ApJ*, 724, 1296.
- Henke, B. L., Gullikson, E. M., & Davis, J. C. 1993, *Atomic Data and Nuclear Data Tables*, 54, 181.
- Juett, A. M., Schulz, N. S., & Chakrabarty, D. 2004, *ApJ*, 612, 308.
- Juett, A. M., Schulz, N. S., Chakrabarty, D., & Gorczyca, T. W. 2006, *ApJ*, 648, 1066.
- Paerels, F. B. S., & Kahn, S. M. 2003, *ARA&A*, 41, 291.
- Palmeri, P., Quinet, P., Mendoza, C., Bautista, M. A., Garcia, J., & Kallman, T. R. 2008, *ApJS*, 177, 408
- Pinto, C., Kaastra, J. S., Costantini, E., & Verbunt, F. 2010, *A&A*, 521, A79
- Schulz, N. S., Nowak, M. A., Chakrabarty, D., & Canizares, C. R. 2010, *ApJ*, 725, 2417
- Smith, F. T. 1960, *Phys. Rev.*, 118, 349.
- Verner, D. A., Yakovlev, D. G., Band, I. M., & Trzhaskovskaya, M. B. 1993, *At. Data Nucl. Data Tables*, 55, 233.
- Witthoeft, M. C., Bautista, M. A., Mendoza, C., Kallman, T. R., Palmeri, P., & Quinet, P. 2009, *ApJS*, 182, 127.
- Witthoeft, M. C., García, J., Kallman, T. R., et al. 2011, *ApJS*, 192, 7

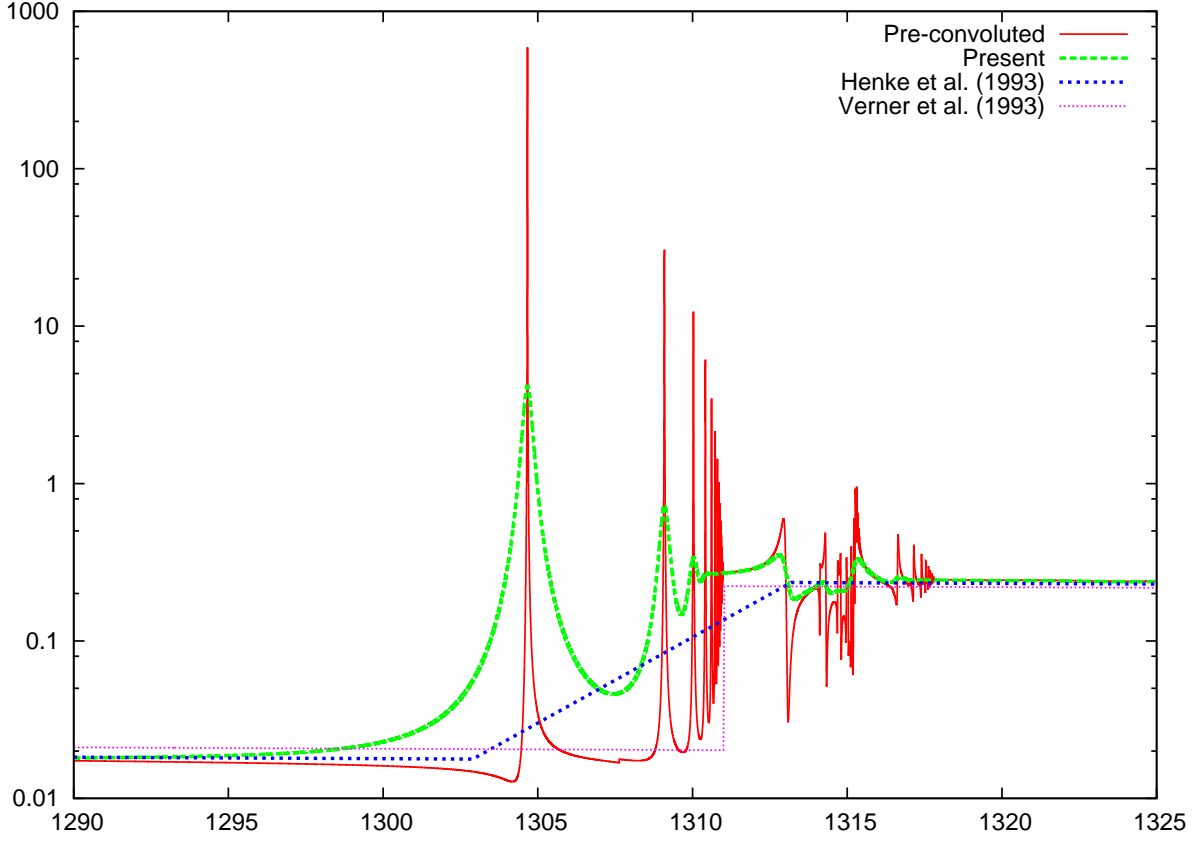


Fig. 1.— Mg I photoabsorption cross sections. Pre-convoluted cross section obtained by damping the core excited states (see Table 1) with a 0.001 Ry, then performing a Lorentzian convolution with the calculated Auger-width of 0.0254 eV for the $1s^2s22p^63s^2 (^2S)$ state (see Table 11) to get the final cross section. Also shown are the IP results (Verner et al. 1993) and solid-state experimental results (Henke et al. 1993).

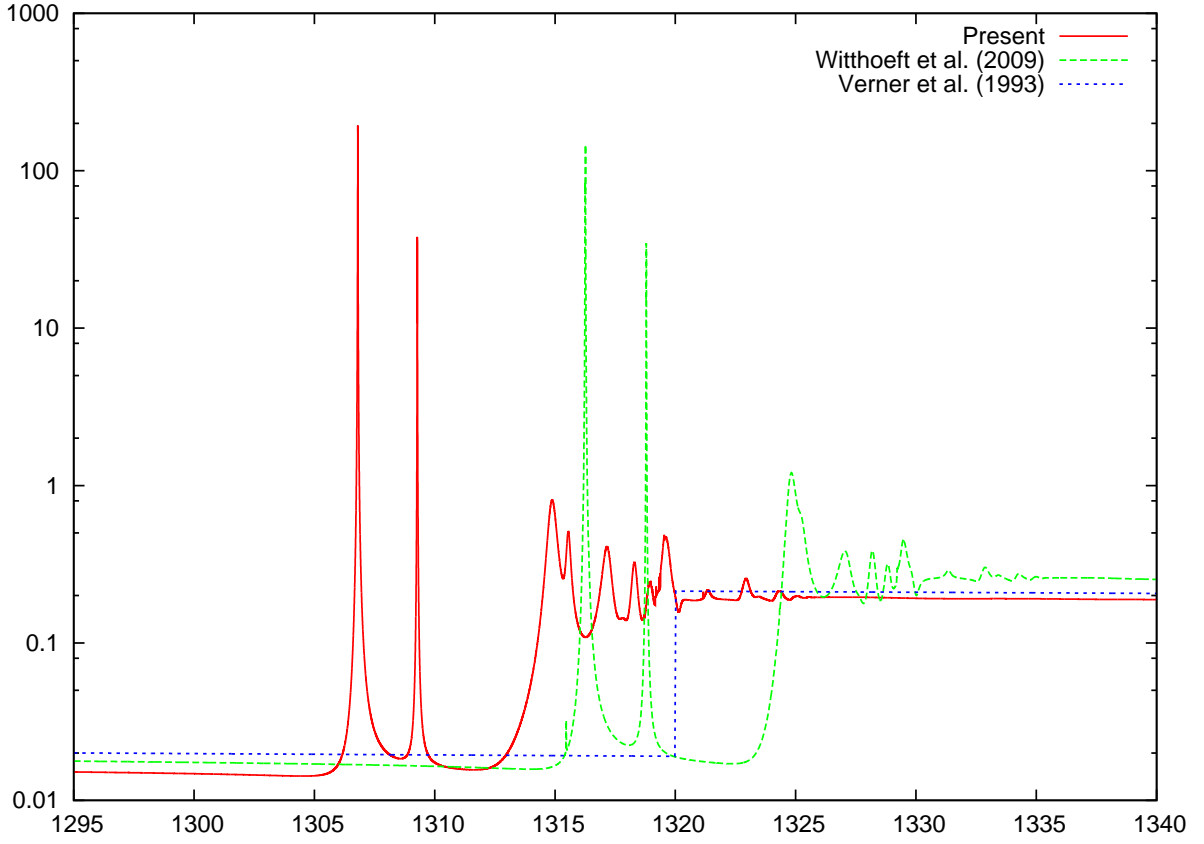


Fig. 2.— Mg II photoabsorption cross sections: present results compared to earlier R-matrix results (Witthoeft et al. 2011) and IP results (Verner et al. 1993).

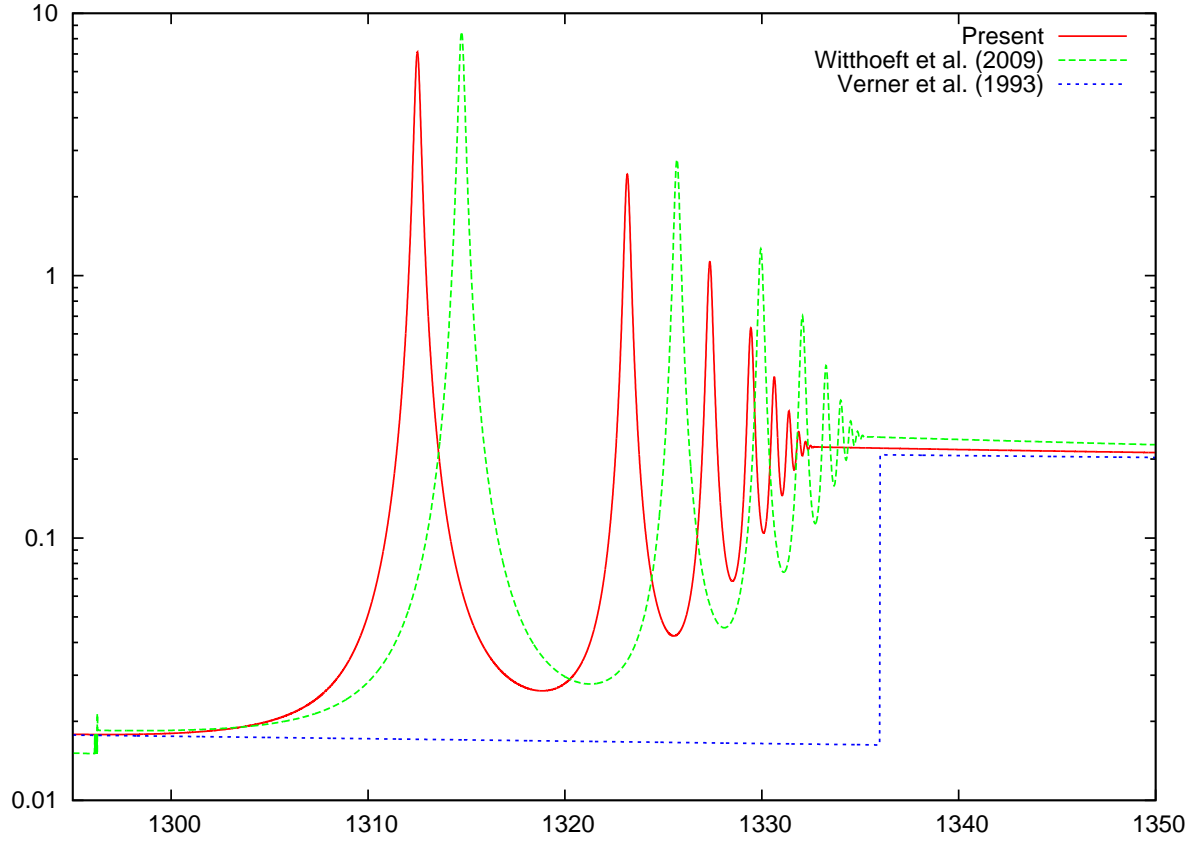


Fig. 3.— Mg III photoabsorption cross sections: present results compared to earlier R-matrix results (Witthoeft et al. 2009) and IP results (Verner et al. 1993).

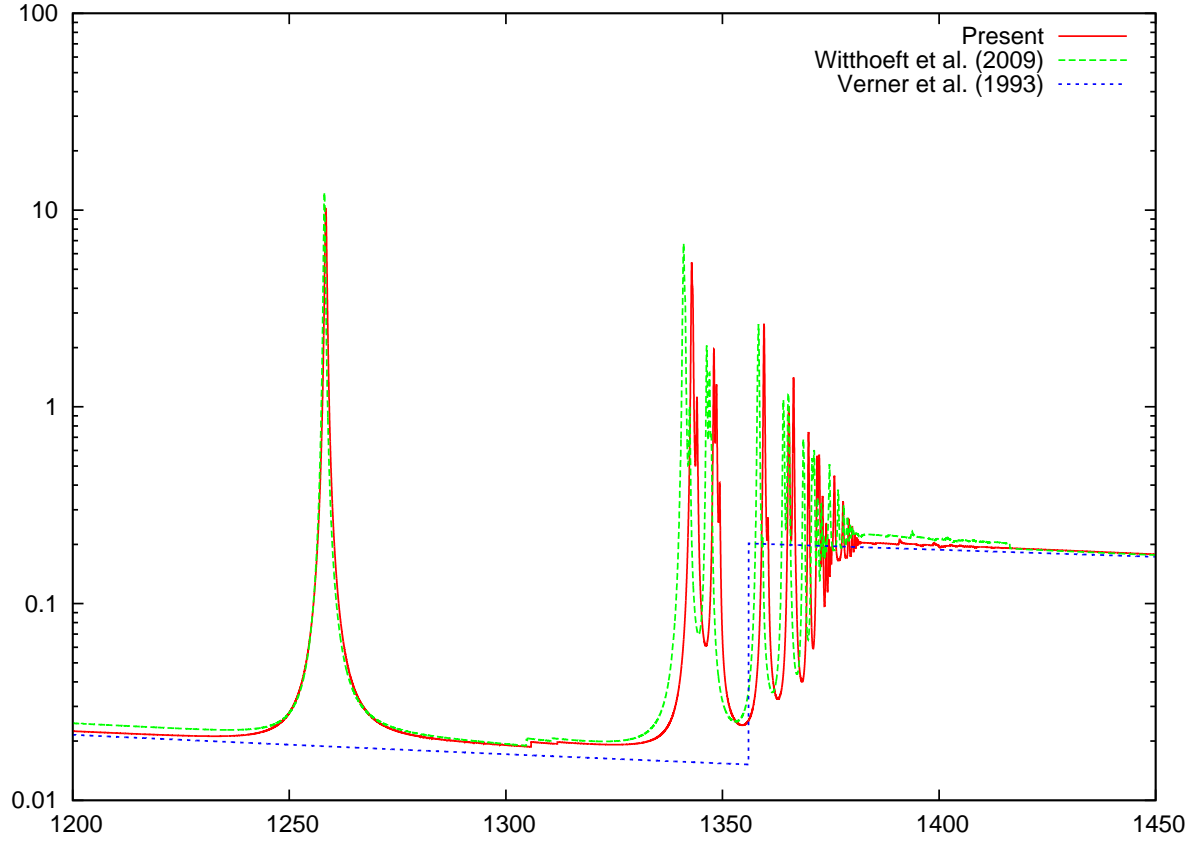


Fig. 4.— Mg IV photoabsorption cross sections: present results compared to earlier R-matrix results (Witthoeft et al. 2009) and IP results (Verner et al. 1993).

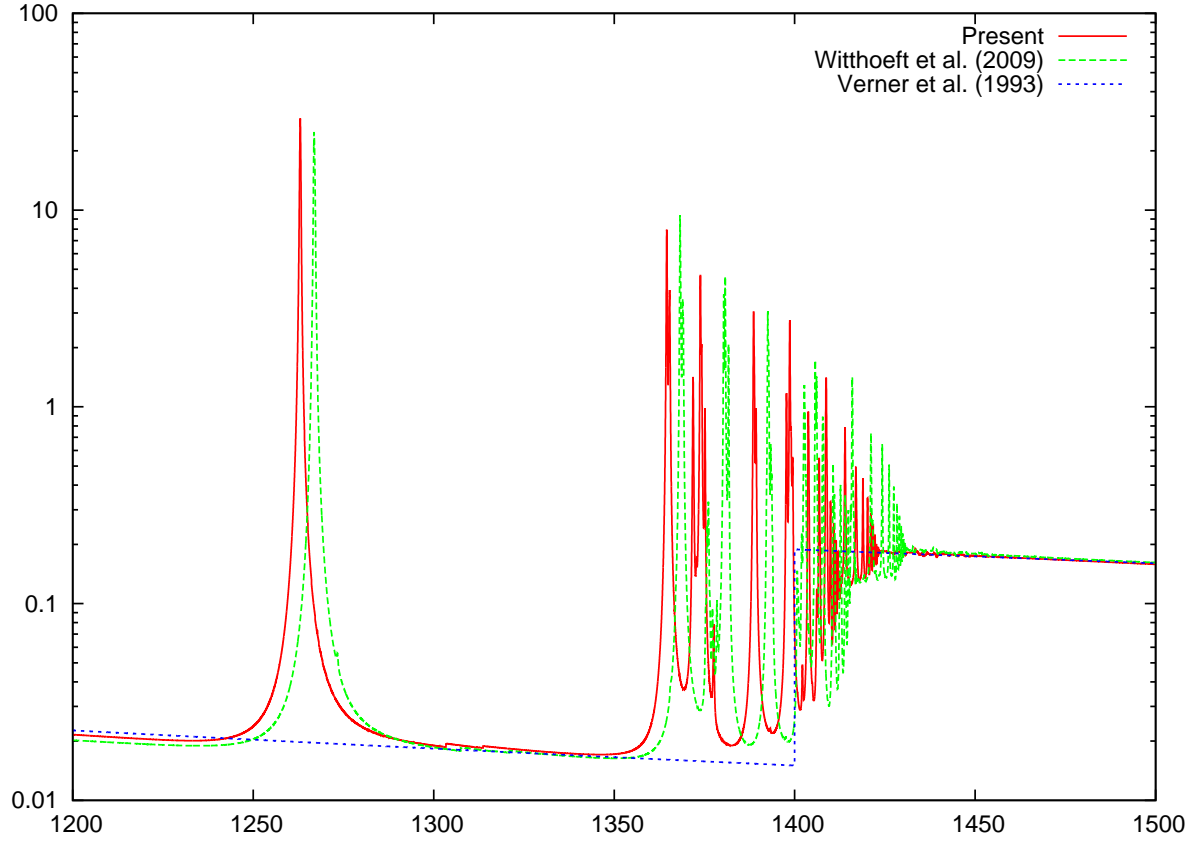


Fig. 5.— Mg V photoabsorption cross sections: present results compared to earlier R-matrix results (Witthoeft et al. 2009) and IP results (Verner et al. 1993).

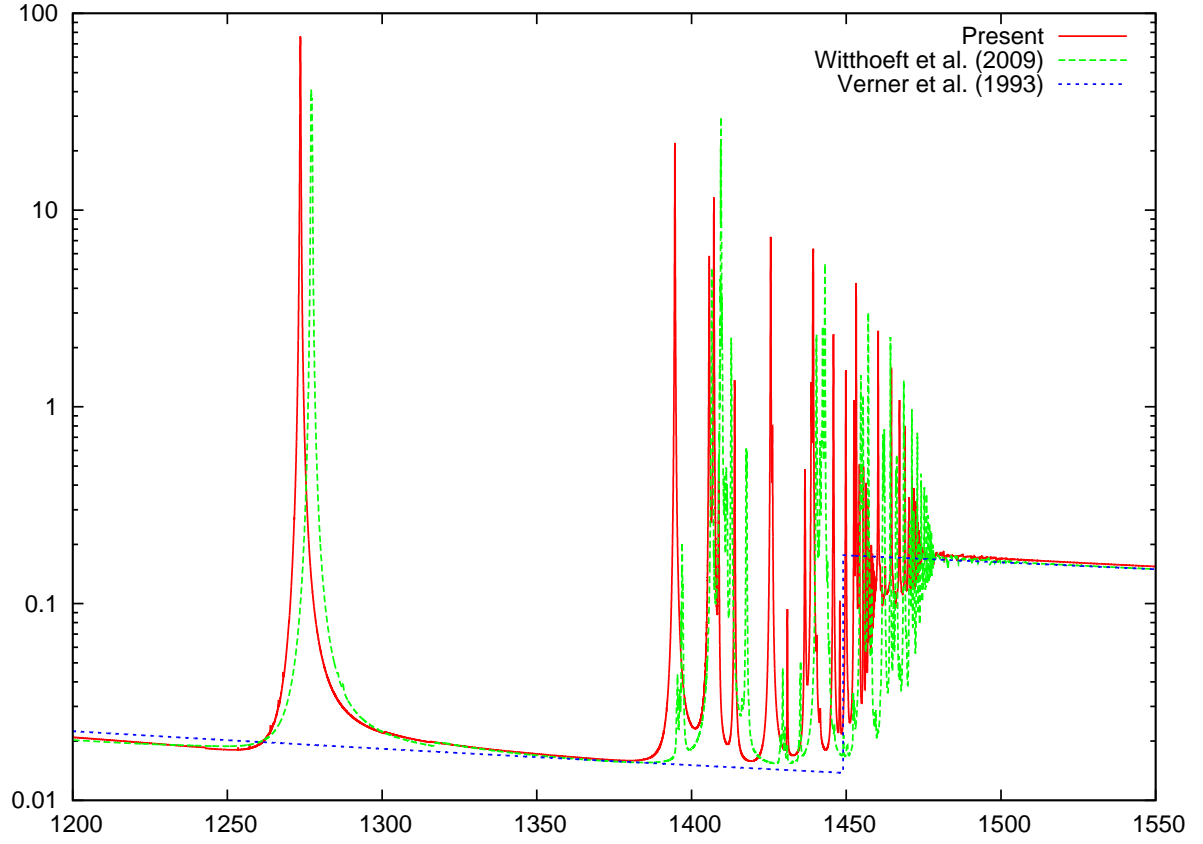


Fig. 6.— Mg VI photoabsorption cross sections: present results compared to earlier R-matrix results (Witthoeft et al. 2009) and IP results (Verner et al. 1993).

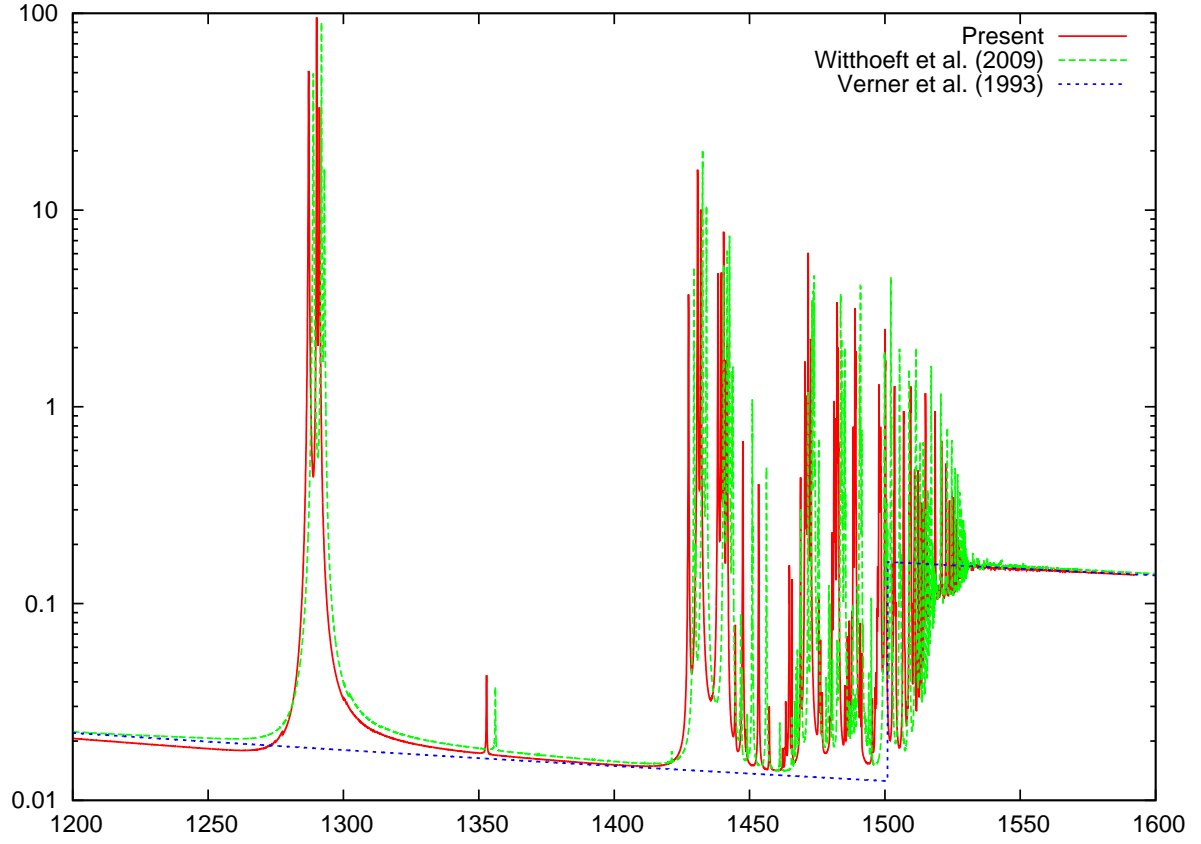


Fig. 7.— Mg VII photoabsorption cross sections: present results compared to earlier R-matrix results (Witthoeft et al. 2009) and IP results (Verner et al. 1993).

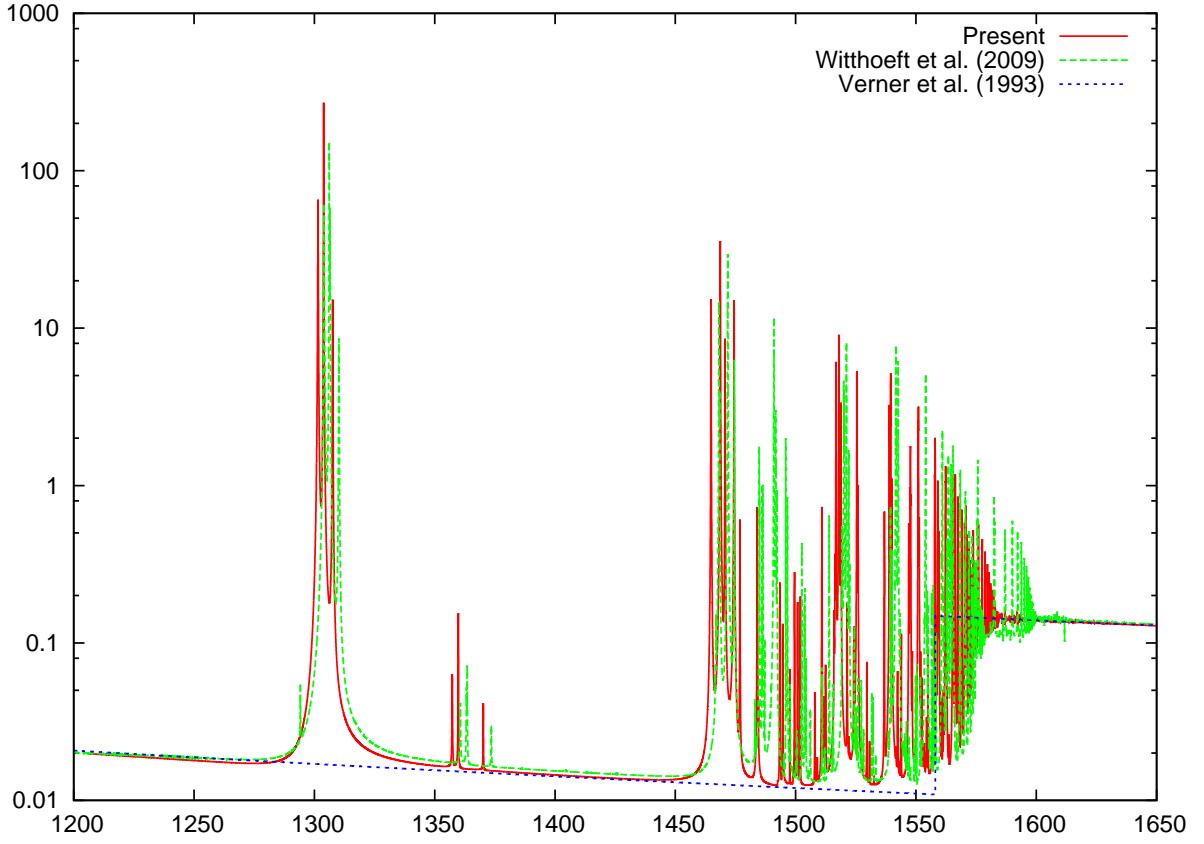


Fig. 8.— Mg VIII photoabsorption cross sections: present results compared to earlier R-matrix results (Witthoeft et al. 2009) and IP results (Verner et al. 1993).

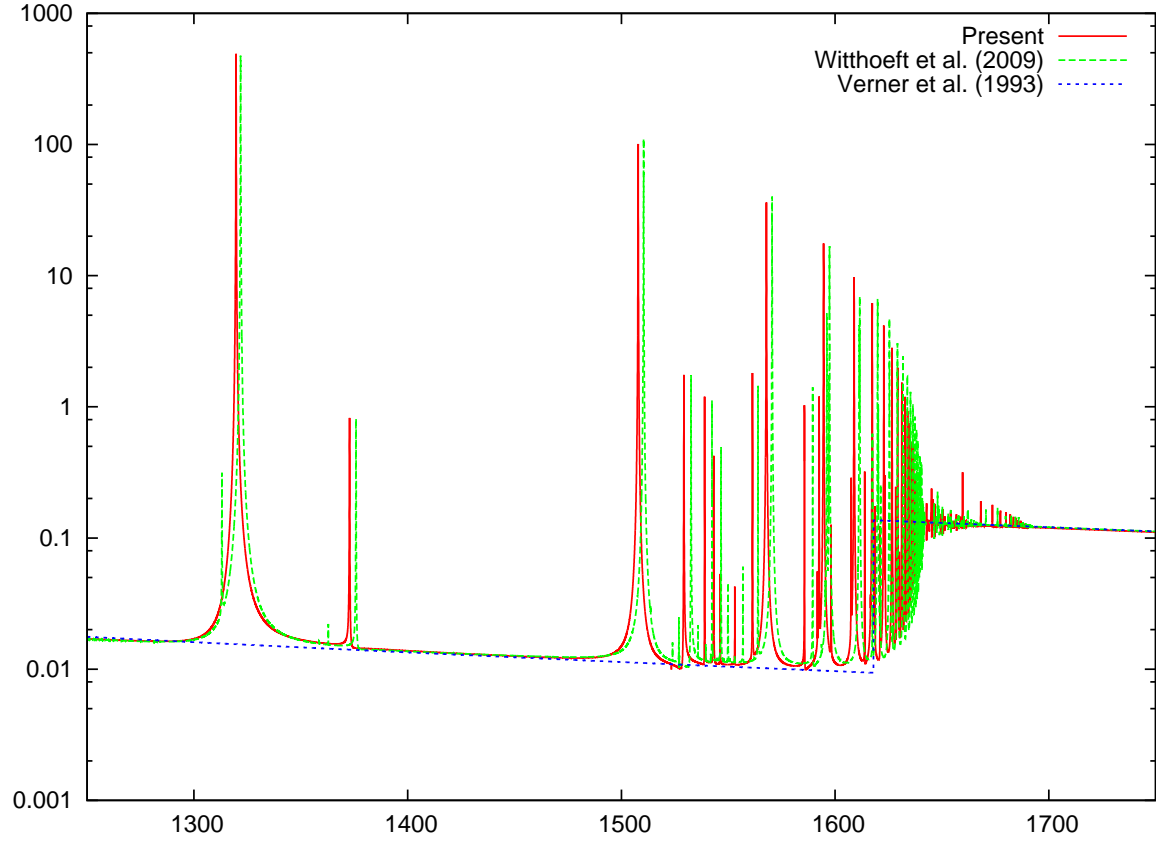


Fig. 9.— Mg IX photoabsorption cross sections: present results compared to earlier R-matrix results (Witthoeft et al. 2009) and IP results (Verner et al. 1993).

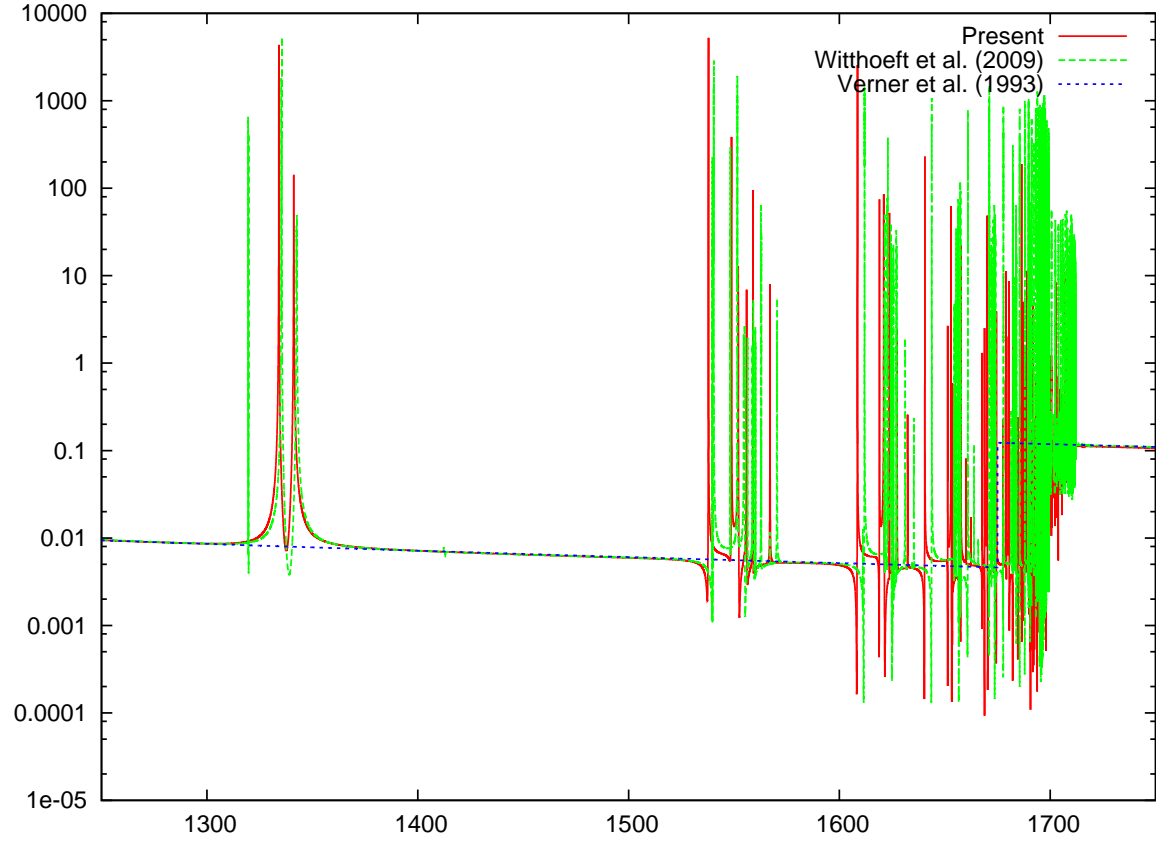


Fig. 10.— Mg X photoabsorption cross sections. Present results compared to earlier R-matrix results (Witthoeft et al. 2009) and IP results (Verner et al. 1993).

Table 1: Energies (in Rydbergs) of the Mg II target states and the Mg I ground state. Also shown are NIST values and HFR1 results (Palmeri et al. 2008).

State	Present	NIST	HFR1
$1s^2 2s^2 2p^6 3s^2 (^1S)$	−0.5428	−0.5620	
$1s^2 2s^2 2p^6 3s (^2S)$	0.0000	0.0000	0.0000
$1s^2 2s^2 2p^6 3p (^2P)$	0.3162	0.3256	0.3300
$1s^2 2s^2 2p^5 3s^2 (^2P)$	3.8240	3.6745	3.6235
$1s^2 2s 2p^6 3s^2 (^2S)$	6.7244		
$1s^2 s 22p^6 3s^2 (^2S)$	95.8157		95.8295
$1s^2 s 22p^6 3s(^1S) 3p (^2P)$	96.1441		96.1612
$1s 2s^2 2p^6 3s(^3S) 3p (^2P)$	96.3185		96.5066

Table 2: Energies (in Rydbergs) of the Mg III target states and the Mg II ground state.

State	Present	NIST
$1s^2 2s^2 2p^6 3s (^2S)$	−1.0928	−1.1051
$1s^2 2s^2 2p^6 (^1S)$	0.0000	0.0000
$1s^2 2s^2 2p^5 3s (^3P)$	3.8897	3.8847
$1s^2 2s^2 2p^5 3s (^1P)$	3.9384	3.9324
$1s^2 2s^2 2p^5 3p (^3S)$	4.2561	4.2591
$1s^2 2s^2 2p^5 3p (^1P)$	4.3615	4.3593
$1s^2 2s^2 2p^5 3p (^3P)$	4.3624	4.3658
$1s^2 2s^2 2p^5 3p (^1S)$	4.5778	4.5200
$1s^2 2s^2 2p^5 3d (^3P)$	4.8345	4.8360
$1s^2 2s^2 2p^5 3d (^1P)$	4.8821	4.8858
$1s^2 2s 2p^6 3s (^3S)$	6.7391	
$1s^2 2s 2p^6 3s (^1S)$	6.8192	
$1s^2 2s 2p^6 3p (^3P)$	7.1714	
$1s^2 2s 2p^6 3p (^1P)$	7.2026	7.204
$1s 2s^2 2p^6 3s (^3S)$	95.9528	
$1s 2s^2 2p^6 3s (^1S)$	96.0030	
$1s 2s^2 2p^6 3p (^3P)$	96.3928	
$1s 2s^2 2p^6 3p (^1P)$	96.4199	

Table 3: Energies (in Rydbergs) of the Mg IV target states and the Mg III ground state.

State	Present	NIST
$1s^2 2s^2 2p^6 (^1S)$	−6.0727	−5.8955
$1s^2 2s^2 2p^5 (^2P)$	0.0000	0.0000
$1s^2 2s 2p^6 (^2S)$	2.6694	2.8321
$1s 2s^2 2p^6 (^2S)$	91.9430	

Table 4: Energies (in Rydbergs) of the Mg V target states and the Mg IV ground state.

State	Present	NIST
$1s^2 2s^2 p^5 (^2P)$	−8.2847	−8.0471
$1s^2 2s^2 p^4 (^3P)$	0.0000	0.0000
$1s^2 2s^2 p^4 (^1D)$	0.3369	0.3194
$1s^2 2s^2 p^4 (^1S)$	0.7227	0.6963
$1s^2 2s^2 p^5 (^3P)$	2.3940	2.5803
$1s^2 2s^2 p^5 (^1P)$	3.4698	3.6142
$1s^2 2p^6 (^1S)$	5.9444	6.0335
$1s 2s^2 2p^5 (^3P)$	92.9165	
$1s 2s^2 2p^5 (^1P)$	93.3603	
$1s 2s 2p^6 (^3S)$	95.3646	
$1s 2s 2p^6 (^1S)$	96.0868	

Table 5: Energies (in Rydbergs) of the Mg VI target states and the Mg V ground state.

State	Present	NIST
$1s^2 2s^2 p^4 (^3P)$	-10.3562	-10.3880
$1s^2 2s^2 2p^3 (^4S)$	0.00000	0.0000
$1s^2 2s^2 2p^3 (^2D)$	0.52952	0.5045
$1s^2 2s^2 2p^3 (^2P)$	0.79048	0.7654
$1s^2 2s 2p^4 (^4P)$	2.24151	2.2682
$1s^2 2s 2p^4 (^2D)$	3.12096	3.1144
$1s^2 2s 2p^4 (^2S)$	3.67859	3.6617
$1s^2 2s 2p^4 (^2P)$	3.90098	3.8805
$1s^2 2p^5 (^2P)$	5.92479	5.9482
$1s 2s^2 2p^4 (^4P)$	93.60545	
$1s 2s^2 2p^4 (^2D)$	94.23068	
$1s 2s^2 2p^4 (^2P)$	94.36199	
$1s 2s^2 2p^4 (^2S)$	94.61941	
$1s 2s 2p^5 (^3P) (^4P)$	95.82506	
$1s 2s 2p^5 (^3P) (^2P)$	96.70406	
$1s 2s 2p^5 (^1P) (^2P)$	97.27956	
$1s 2p^6 (^2S)$	99.41050	

Table 6: Energies (in Rydbergs) of the Mg VII target states and the Mg VI ground state.

State	Present	NIST
$1s^2 2s^2 2p^3 (^4S)$	-13.7208	-13.7260
$1s^2 2s^2 2p^2 (^3P)$	0.0000	0.0000
$1s^2 2s 2p^3 (^5S)$	1.0016	1.0580
$1s^2 2s 2p^3 (^3D)$	2.0873	2.1044
$1s^2 2s 2p^3 (^3P)$	2.4774	2.4870
$1s^2 2s 2p^3 (^3S)$	3.2739	3.2817
$1s^2 2p^4 (^3P)$	4.8865	4.9331
$1s 2s^2 2p^3 (^5S)$	93.6369	
$1s 2s^2 2p^3 (^3D)$	94.4994	
$1s 2s^2 2p^3 (^3S)$	94.7250	
$1s 2s^2 2p^3 (^3P)$	94.7628	
$1s 2s 2p^4 (^5P)$	95.4771	
$1s 2s 2p^4 (^4P) (^3P)$	96.6606	
$1s 2s 2p^4 (^3D)$	96.6883	
$1s 2s 2p^4 (^3S)$	97.3056	
$1s 2s 2p^4 (^2P) (^3P)$	97.5790	
$1s 2p^5 (^3P)$	99.2593	

Table 7: Energies (in Rydbergs) of the Mg VIII target states and the Mg VII ground state.

State	Present	NIST
$1s^2 2s^2 2p^2 (^3P)$	−16.6018	−16.5380
$1s^2 2s^2 2p (^2P)$	0.0000	0.0000
$1s^2 2s 2p^2 (^4P)$	1.0960	1.1799
$1s^2 2s 2p^2 (^2D)$	2.0518	2.0967
$1s^2 2s 2p^2 (^2S)$	2.7119	2.6981
$1s^2 2s 2p^2 (^2P)$	2.8492	2.8965
$1s^2 2p^3 (^4S)$	3.6653	3.7490
$1s^2 2p^3 (^2D)$	4.1728	4.2244
$1s^2 2p^3 (^2P)$	4.7639	4.7621
$1s 2s^2 2p^2 (^4P)$	94.9623	
$1s 2s^2 2p^2 (^2D)$	95.6660	
$1s 2s^2 2p^2 (^2P)$	95.8214	
$1s 2s^2 2p^2 (^2S)$	96.0915	
$1s 2s 2p^3 (^4D)$	96.5601	
$1s 2s 2p^3 (^4S)$	96.6315	
$1s 2s 2p^3 (^4P)$	97.0167	
$1s 2s 2p^3 (^2D)$	97.5622	
$1s 2s 2p^3 (^4S)$	97.8941	
$1s 2s 2p^3 (^2P)$	98.0187	
$1s 2s 2p^3 (^2D)$	98.1266	
$1s 2s 2p^3 (^2P)$	98.5930	
$1s 2s 2p^3 (^2S)$	98.6195	
$1s 2p^4 (^4P)$	99.0702	
$1s 2p^4 (^2D)$	99.7024	
$1s 2p^4 (^2P)$	99.8864	
$1s 2p^4 (^2S)$	100.6505	

Table 8: Energies (in Rydbergs) of the Mg IX target states and the Mg VIII ground state.

State	Present	NIST
$1s^2 2s^2 2p (^2P)$	−19.5175	−19.5450
$1s^2 2s^2 (^1S)$	0.0000	0.0000
$1s^2 2s 2p (^3P)$	1.2720	1.3020
$1s^2 2s 2p (^1P)$	2.4716	2.4758
$1s^2 2p^2 (^3P)$	3.3112	3.3555
$1s^2 2p^2 (^1D)$	3.6698	3.6915
$1s^2 2p^2 (^1S)$	4.6220	4.5530
$1s 2s^2 2p (^3P)$	96.3470	
$1s 2s^2 2p (^1P)$	96.9743	97.1192
$1s 2s (^3S) 2p^2 (^3D)$	97.9274	
$1s 2s (^1S) 2p^2 (^3P)$	97.9575	
$1s 2s (^3S) 2p^2 (^3S)$	98.6507	
$1s 2s (^3S) 2p^2 (^1D)$	98.7677	
$1s 2s (^3S) 2p^2 (^3P)$	98.8326	
$1s 2s (^3S) 2p^2 (^1P)$	99.3433	
$1s 2s (^1S) 2p^2 (^1S)$	99.4907	
$1s 2p^3 (^3D)$	99.6064	
$1s 2p^3 (^3S)$	99.9059	
$1s 2p^3 (^1D)$	100.1887	
$1s 2p^3 (^3P)$	100.2962	
$1s 2p^3 (^1P)$	100.8812	

Table 9: Energies (in Rydbergs) of the Mg X target states and the Mg IX ground state.

State	Present	NIST
$1s^2 2s^2 (^1S)$	-24.0872	-24.1060
$1s^2 2s (^2S)$	0.0000	0.0000
$1s^2 2p (^2P)$	1.4855	1.4823
$1s 2s^2 (^2S)$	96.4886	
$1s 2s (^1S) 2p (^2P)$	97.9741	98.1544
$1s 2s (^3S) 2p (^2P)$	98.5011	98.6810
$1s 2p^2 (^2D)$	99.0911	99.2730
$1s 2p^2 (^2P)$	99.3072	99.5100
$1s 2p^2 (^2S)$	100.2157	100.310

Table 10: Energies (in Rydbergs) of the Mg XI target states and the Mg X ground state.

State	Present	NIST
$1s^2 2s (^2S)$	-26.9543	-27.0100
$1s^2 (^1S)$	0.0000	0.0000
$1s 2s (^3S)$	97.6959	97.8349
$1s 2p (^3P)$	98.5492	98.7331
$1s 2s (^1S)$	98.6309	98.7702
$1s 2p (^1P)$	99.2148	99.3884

Table 11: Present Auger widths (in eV) for the 3 Mg II autoionizing target states above the K-shell threshold (see Table 1). Also shown are the level-averaged HFR1 results (Palmeri et al. 2008).

	State	Present	HFR1
1	$1s^2s22p^63s^2(^2S)$	$2.54E-02$	$2.39E-02$
2	$1s^2s22p^63s(^1S)3p(^2P)$	$1.73E-02$	$2.37E-02$
3	$1s2s^22p^63s(^3S)3p(^2P)$	$2.26E-02$	$2.36E-02$

Table 12: Present Auger widths (in eV) for the 4 Mg III autoionizing target states above the K-shell threshold (see Table 2). Also shown are the level-averaged HFR1 results (Palmeri et al. 2008).

	State	Present	MCBP
1	$1s2s^22p^63s\ (^3S)$	$2.39E-02$	$2.68E-02$
2	$1s2s^22p^63s\ (^1S)$	$2.41E-02$	$2.52E-02$
3	$1s2s^22p^63p\ (^3P)$	$2.37E-02$	$2.45E-02$
4	$1s2s^22p^63p\ (^1P)$	$2.33E-02$	$2.44E-02$

Table 13: Present Auger widths (in eV) for the Mg IV autoionizing target state above the K-shell threshold (see Table 5). Also shown are level-averaged HFR1 widths (Palmeri et al. 2008) and AUTOSTRUCTURE results (Gorczyca et al. 2003).

State	Present	HFR1	AUTO
$1s2s^22p^6(^2S)$	$2.45E - 02$	$2.45E - 03$	$3.01E - 02$

Table 14: Present Auger widths (in eV) for the 4 Mg V autoionizing target states above the K-shell threshold (see Table 4). Also shown is the level-averaged results (Palmeri et al. 2008).

	State	Present	MCBP
1	$1s2s^22p^5(^3P)$	$2.13E-02$	$2.22E-02$
2	$1s2s^22p^5(^1P)$	$2.02E-02$	$2.06E-02$
3	$1s2s2p^6(^3S)$	$1.90E-02$	$2.00E-02$
4	$1s2s2p^6(^1S)$	$2.84E-02$	$3.05E-02$

Table 15: Present Auger widths (in eV) for the 8 Mg VI autoionizing target states above the K-shell threshold (see Table 5). Also shown are the level-averaged HFR1 results (Palmeri et al. 2008).

	State	Present	HFR1
1	$1s2s^22p^4 (^4P)$	$1.66E - 02$	$1.64E - 02$
2	$1s2s^22p^4 (^2D)$	$2.00E - 02$	$1.96E - 02$
3	$1s2s^22p^4 (^2P)$	$1.45E - 02$	$1.39E - 02$
4	$1s2s^22p^4 (^2S)$	$1.87E - 02$	$1.83E - 02$
5	$1s2s2p^5(^3P) (^4P)$	$1.49E - 02$	$1.46E - 02$
6	$1s2s2p^5(^3P) (^2P)$	$1.97E - 02$	$1.89E - 02$
7	$1s2s2p^5(^1P) (^2P)$	$2.02E - 02$	$2.03E - 02$
8	$1s2p^6 (^2S)$	$1.89E - 02$	$1.87E - 02$

Table 16: Present Auger widths (in eV) for the 10 Mg VII autoionizing target states above the K-shell threshold (see Table 6). Also shown are level-averaged HFR1 (Palmeri et al. 2008), level-averaged MCBP (Hasoğlu et al. 2008), and level-averaged MCDF (Hasoğlu et al. 2008) widths.

	State	Present	HFR1	MCDF	MCBP
1	$1s2s^22p^3 (^5S)$	$9.31E-03$	$9.53E-03$	$1.36E-02$	$9.95E-03$
2	$1s2s^22p^3 (^3D)$	$1.54E-02$	$1.53E-02$	$1.91E-02$	$1.59E-02$
3	$1s2s^22p^3 (^3S)$	$5.82E-03$	$5.52E-03$	$8.89E-03$	$5.72E-03$
4	$1s2s^22p^3 (^3P)$	$1.45E-02$	$1.40E-02$	$1.77E-02$	$1.46E-02$
5	$1s2s2p^4 (^5P)$	$8.57E-03$	$8.56E-03$		
6	$1s2s2p^4 (^4P) (^3P)$	$1.18E-02$	$1.15E-02$		
7	$1s2s2p^4 (^3D)$	$1.37E-02$	$1.36E-02$		
8	$1s2s2p^4 (^3S)$	$1.10E-02$	$1.08E-02$		
9	$1s2s2p^4 (^2P) (^3P)$	$1.50E-02$	$1.51E-02$		
10	$1s2p^5 (^3P)$	$1.46E-02$	$1.48E-02$		

Table 17: Present Auger widths (in eV) for the 17 Mg VIII autoionizing target states above the K-shell threshold (see Table 7). Also shown are level-averaged HFR1 (Palmeri et al. 2008), level-averaged MCDF (Chen & Craseman 1988), and level-averaged MCBP (Hasoğlu et al. 2006) widths.

	State	Present	HFR1	MCDF	MCBP
1	$1s2s^22p^2 (^4P)$	$8.73E-03$	$7.81E-03$	$8.98E-03$	$9.06E-03$
2	$1s2s^22p^2 (^2D)$	$1.30E-02$	$1.23E-02$	$1.27E-02$	$1.30E-02$
3	$1s2s^22p^2 (^2P)$	$5.63E-03$	$4.60E-03$	$5.37E-03$	$5.32E-03$
4	$1s2s^22p^2 (^2S)$	$1.15E-02$	$1.00E-02$	$1.12E-02$	$1.11E-02$
5	$1s2s(^3S)2p^3 (^4D)$	$8.35E-03$	$8.71E-03$	$8.17E-03$	
6	$1s2s(^1S)2p^3 (^4S)$	$1.46E-03$	$6.92E-04$	$1.91E-03$	
7	$1s2s(^3S)2p^3 (^4P)$	$6.40E-03$	$6.63E-03$	$6.28E-03$	
8	$1s2s(^1S)2p^3 (^2D)$	$1.13E-02$	$1.06E-02$	$1.15E-02$	
9	$1s2s(^3S)2p^3 (^4S)$	$7.63E-03$	$6.97E-03$	$8.51E-03$	
10	$1s2s(^1S)2p^3 (^2P)$	$9.45E-03$	$8.45E-03$	$9.59E-03$	
11	$1s2s(^3S)2p^3 (^2D)$	$1.33E-02$	$1.30E-02$	$1.39E-02$	
12	$1s2s(^3S)2p^3 (^2P)$	$1.14E-02$	$1.07E-02$	$1.16E-02$	
13	$1s2s(^3S)2p^3 (^2S)$	$2.86E-03$	$3.71E-03$	$3.41E-03$	
14	$1s2p^4 (^4P)$	$8.38E-03$	$6.48E-03$	$8.73E-03$	
15	$1s2p^4 (^2D)$	$1.33E-02$	$1.01E-02$	$1.37E-02$	
16	$1s2p^4 (^2P)$	$8.34E-03$	$6.47E-03$	$8.58E-03$	
17	$1s2p^4 (^2S)$	$9.18E-03$	$6.72E-03$	$9.48E-03$	

Table 18: Present Auger widths (in eV) for the Mg IX autoionizing target states above the K-shell threshold (see Table 8). Also shown are level-averaged HFR1 (Palmeri et al. 2008), level-averaged MCDF (Chen 1985) and level-averaged MBCP (Gorczyca et al. 2003) widths.

	State	Present	HFR1	MCDF	MCBP
1	$1s2s^22p(^3P)$	$7.44E-03$	$7.35E-03$	$7.61E-03$	$7.89E-03$
2	$1s2s^22p(^1P)$	$5.26E-03$	$4.84E-03$	$5.08E-03$	$5.12E-03$
3	$1s2s(^3S)2p^2(^3D)$	$6.62E-03$	$5.95E-03$	$5.87E-03$	
4	$1s2s(^1S)2p^2(^3P)$	$8.51E-04$	$2.30E-03$	$2.01E-03$	
5	$1s2s(^3S)2p^2(^3S)$	$3.36E-03$	$3.29E-03$	$3.10E-03$	
6	$1s2s(^3S)2p^2(^1D)$	$1.12E-02$	$1.17E-02$	$1.23E-02$	
7	$1s2s(^3S)2p^2(^3P)$	$6.06E-03$	$6.27E-03$	$6.40E-03$	
8	$1s2s(^3S)2p^2(^1P)$	$2.44E-03$	$2.16E-03$	$1.89E-03$	
9	$1s2s(^1S)2p^2(^1S)$	$8.24E-03$	$8.03E-03$	$8.76E-03$	
10	$1s2p^3(^3D)$	$8.43E-03$	$8.80E-03$	$8.50E-03$	
11	$1s2p^3(^3S)$		$1.14E-05$	$1.49E-05$	
12	$1s2p^3(^1D)$	$8.39E-03$	$8.61E-03$	$8.27E-03$	
13	$1s2p^3(^3P)$	$5.32E-03$	$5.53E-03$	$5.31E-03$	
14	$1s2p^3(^1P)$	$5.05E-03$	$5.27E-03$	$5.03E-03$	

Table 19: Present Auger widths (in eV) for the Mg X autoionizing target states above the K-shell threshold (see Table 5). Also shown are level-averaged HFR1 (Palmeri et al. 2008), level-averaged MCDF(Chen 1986), and level-averaged MBCP (Gorczyca et al. 2006) widths.

	State	Present	HFR1	MCDF	MCBP
1	$1s2s^2(^2S)$	$6.27E-03$	$5.81E-03$	$5.42E-03$	$6.28E-03$
2	$1s2s(^1S)2p(^2P)$	$4.06E-03$	$4.02E-03$	$3.53E-03$	
3	$1s2s(^3S)2p(^2P)$	$2.89E-04$	$3.21E-04$	$5.44E-04$	
4	$1s2p^2(^2D)$	$6.39E-03$	$6.90E-03$	$6.61E-03$	
5	$1s2p^2(^2P)$		$3.98E-05$	$3.37E-05$	
6	$1s2p^2(^2S)$	$9.41E-04$	$1.05E-03$	$1.10E-03$	